Silver nitrate *in situ* Upgrades Pyrolysis Biofuels from Brewer's Spent Grain via Biotemplating

Cole H. Ashman[1], Lihui Gao[1,2], Jillian L. Goldfarb,[1,3]*

1. Department of Mechanical Engineering, Boston University, 110 Cummington Mall, Boston MA 02215, United States
2. School of Chemical Engineering and Technology, China University of Mining and Technology, No 1 Daxue Road Xuzhou 221116, People's Republic of China
3. Department of Biological and Environmental Engineering, Cornell University, 226 Riley-Robb Hall, Ithaca NY 14853

Abstract

Bio-based hydrocarbon fuels made from carbonaceous wastes are a renewable and potentially carbon neutral alternative to conventional fossil fuels. Pyrolysis biofuels are limited largely because of a poor overall energy balance along with the fuel's high viscosity and high oxygen content. This study explores an integrated biorefinery approach to manage Brewer's Spent Grain (BSG) waste that combines *in situ* catalytic upgrading of pyrolysis fuel with production of value-added products to improve process economics. By incorporating silver nitrate via a wet impregnation method into BSG prior to pyrolysis, non-condensable gas (particularly hydrogen and ethane) production dramatically increases, while the evolution of methane is largely unchanged. Critically, the peak temperatures at which pyrolysis gases evolve are decreased by the incorporation of silver, suggesting that this process could lower required pyrolysis temperatures. The silver-treated pyrolysis bio-oil showed a considerable increase in furfural, an important precursor in many chemical processes. The silver-impregnated biomass also showed a decrease in 2-methyl-propanal and 2-methyl-butanal yields, and virtually eliminated detectable anthracene and pyrene. In conjunction with the evolved gas results, it is likely that molecular rearrangement and dehydrogenation pathways, as opposed to a complete thermochemical cracking of the bio-oil fraction, are likely responsible for the catalytic behavior observed. After pyrolysis, the biochar can be oxidized to yield bio-templated, green-synthesized silver micro- and nanomaterials. The integrated biorefinery approach offers a novel path for upgrading pyrolysis biofuels, unifying synthesis of micro- and nanostructured materials and fuel production.

Keywords

Integrated biorefinery; brewer's spent grain; *in situ* upgrading; biotemplate; pyrolysis; metal impregnation

* To whom correspondence should be addressed: (607) 255 5789; JillianLGoldfarb@gmail.com; goldfarb@cornell.edu

Graphical Abstract

Pyrolysis biofuels can be in situ upgraded by impregnation with catalyst precursors, simultaneously forming biotemplated materials, enhancing hydrogen production and decreasing oxygenated compounds in condensable bio-oil

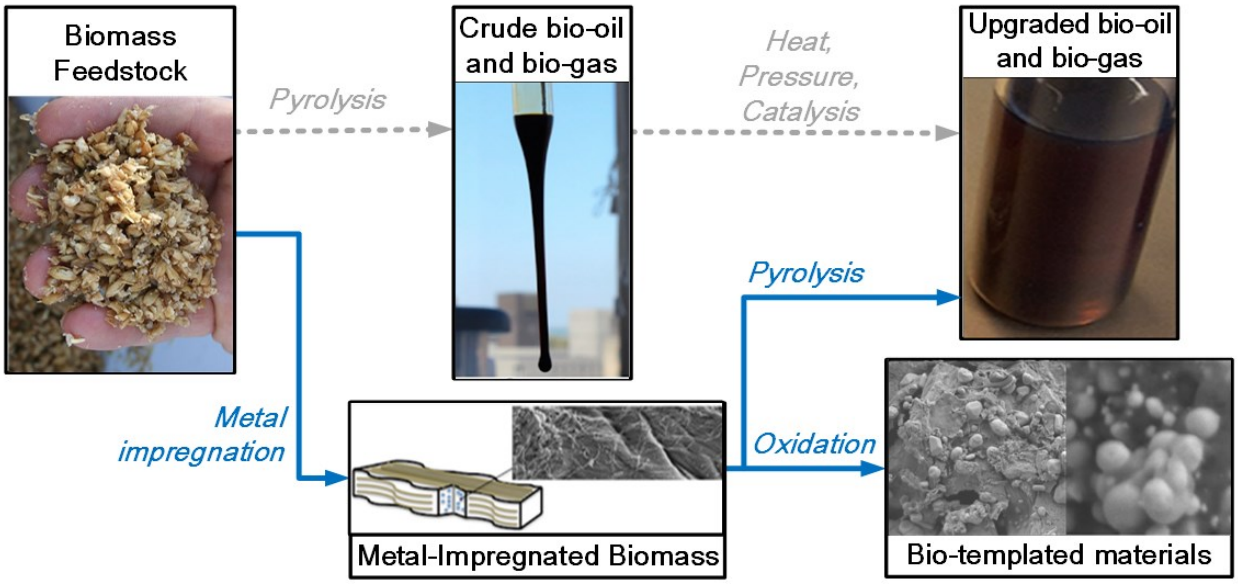

1. Introduction

The global demand for sustainable, reliable sources of energy is steadily growing as developing nations expand and world population rises. As this trend continues it is imperative that we work to curb our reliance on non-renewable fossil energy sources, which are inextricably linked to climate change and environmental degradation. One potential alternative to fossil fuels is pyrolysis biofuels derived from lignocellulosic biomasses from agricultural and food waste streams. While biofuel derived from biomass is attractive as a potential renewable, sustainable, and comparatively carbon-neutral energy source, it has received considerable scrutiny over the years on the basis of the overall process' energy balance and economics, as well as net environmental impact[1,2]. These criticisms may be countered, in part, by recovering both fuels and additional value-added products[3–6].

Perhaps the most significant issue with the production of biofuels from biomass via pyrolysis (heating in the absence of oxygen) is the relatively poor quality of the liquid bio-oil product. This bio-oil tends to be both acidic and high in oxygen content, leading to corrosion in engines and process units. It also renders the fuels prone to degradation over time[7]. Bio-oil upgrading via both physical and chemical treatment has been investigated by many, from *in situ* and downstream chemical catalysts[8] to solvent-free mechanocatalytic processes using sacrificial catalysts[9]. Nevertheless, challenges persist such as the presence of viscous, oxygenated polar compounds which are subject to polymerization at temperatures as low as 120°C and are largely responsible for the fuel's thermal instability[10,11]. In short, poor fuel quality and yield, along with the relatively high cost of fuel upgrading processes — particularly with respect to catalyst degradation and recovery[12] — has stymied large-scale development and adoption of this type of biofuel[13]. However, biomass-to-biofuel processes may be bolstered both in terms of process economics and fuel quality by pursuing an *integrated biorefinery* approach.

The incorporation of pre-formed nanomaterials into biomass to catalyze biofuel production has been explored throughout the biofuel literature. First-generation biofuels have profited greatly from nanomaterial catalysts, from improved transesterification of bio-oils using nano- Fe_3O_4, CaO, and γ-Al_2O_3[14,15], to conversion of glycol to high-value chemical products using ZnO supported Rh and Pt[6]. This extends to second-generation biofuels from lignocellulosic and agricultural waste

streams. For example, Ni-W catalysts increase yield of ethylene glycol, and Ru can increase sorbitol, isosorbide, and hexitol yields in bio-oils[16–20]. Ti and Al nano-catalysts demonstrated potential in improving levoglucosan yield in cellulose and anhydrous sugar pyrolysis[21,22], and sulfated metal oxides improved yield of light furans from cellulose pyrolysis[23]. Nano-NiO on γ-Al_2O_3 has been explored for upgrading pyrolysis gases and tar removal[21], while incorporation of nano-SnO_2 particles into hazelnut shell biomass catalyzed pyrolysis and increased biogas generation[24]. Catalysts naturally found in red mud were also shown to enhance components of fast pyrolysis, particularly with respect to ketone yield[25]. Still others have studied the efficacy of *in situ* upgrading of pyrolysis products by incorporating zeolites into biomass prior to pyrolysis[26]. These examples and many more clearly demonstrate the benefit of catalyst integration into the biomass-to-biofuel process.

In the present work, brewer's spent grain (BSG) was used as feedstock for *in situ* catalyzed biofuel production. BSG was selected due to its potential scalability/availability as a biomass, and its dissimilarity to the pure cellulose feedstock previously examined by our laboratory[27] and the others cited throughout this paper. Silver was chosen as the *in situ* catalyst for several reasons. First, noble and transition metals used as heterogeneous catalysts in thermochemical conversion systems such as gasification and pyrolysis have been shown to decrease operation temperature and increase biomass conversion[27,28]. Ag and Au, more so than Cu, Ni, Ru, Rh, Pd and Pt, have been shown to lower activation energy barriers to CO conversion[29], and transition metals are responsible for catalytic tar elimination during biomass pyrolysis[30] and CO hydrogenation to methanol[31]. Overall, transition metals are responsible for C-C, C-O, C-N, N-O, N-N and O-O dissociation reactions[32], critical to the pyrolysis process. The cost of silver, compared to other transition metals, is considerably lower; early 2019 prices for silver hover around $0.50 per gram, whereas gold was at $41/g, ruthenium at $8/g, palladium at $44/g and platinum at $26/g[33]. Finally, silver micro/nanomaterials as a byproduct could represent a high-value antimicrobial material[34–36].

Another growing body of literature exists surrounding the use of biomass as a template for green synthesis of micro- and nano-structures[37–39]. These processes take advantage of natural organic reducing agents leading to direct nucleation[40] as well as the naturally complex micro- and nano-scale structures present in biological materials[41]. This greener pathway obviates the need for harsh

chemical reductants like hydrazines or sodium borohydride as well as volatile organic solvents while presenting a viable means to produce engineered nanomaterials[42–44]. This process was used to synthesize silver nanoparticles using a number of organic substances including soluble starch[45], plant extracts[46–49], and cellulose as a structure-directing support for production of nanoparticles[50]. Similar bio-templating of inorganic nanomaterials has been shown for titanium[51–53], iron[54–56], and zinc[57–59]. Once these nanomaterials are formed, the organic scaffolding is removed through oxidation in air. Our integrated approach attempts to join bio-templating of ordered micro- and nano-materials as a means itself for catalyzing pyrolysis and upgrading of biofuel components. This paper explores the feasibility of such an integrated biorefinery by simultaneously upgrading pyrolysis biofuel from brewer's spent grain while producing a value-added material, namely bio-templated silver particles, which may be used in medicine, optics, and electrochemistry[60,61]. This paper explores the catalytic upgrading that can be achieved by incorporating a catalyst precursor into the biomass, rather than a previously formed nano- or microstructured catalyst. As such, the paper directly addresses key concepts in Green Engineering for Sustainable Development that can be achieved via pyrolysis, including the development of environmentally improved routes, synthetic methods and processes to achieve key products and chemicals by exploiting the chemical aspects of renewable energy.

2. Experimental

Brewer's spent grain (BSG), the residual barley grain malt and other solids left once the fermentable liquid wort is removed, is the main waste product from the beer brewing process, comprising about 85% of the total waste generated[62]. The composition of BSG varies based on the variety of barley used in fermentation, hops, and other additives. Generally speaking, it is comprised of lignocellulosic biomass high in protein and fiber content, roughly 16 to 25% cellulose, 15 to 24% protein, and 11 to 27% lignin (by dry mass basis)[63,64]. Because of its high protein content, BSG is most commonly used for animal fodder[65,66], though it has been explored for many other uses including as a wastewater adsorbent[67], a growth medium for microorganisms and enzyme production, as well as a feedstock for biochemical compounds such as amino acids and antioxidants[68]. Some have explored the potential for BSG as an energy source, including as a charcoal precursor[69,70], as a feedstock for ethanol[71–73], in production of bio-gas via anaerobic

digestion[74–76], and for the production of pyrolysis biofuels[77,78]. BSG was selected in this work as an attractive biomass feedstock for our process given its low cost, widespread abundance, and large quantity generated each year—approximately 23 kg produced per barrel of beer, with over 200 million barrels produced in the US in 2015[63,65,79].

2.1 Materials

BSG was obtained in bulk from Anheuser Busch (Everett, MA), and dried in an oven overnight at 90 °C to achieve a constant moisture baseline. To ensure studies were not transport limited, biomass particles were reduced to 250-300 μm by ball milling and sieving, which prior work demonstrates yields a Biot number of much less than one[80]. Ultimate analysis was performed using a LECO 628 analyzer equipped with the sulfur module for CHN (ASTM D-5373 standard method) and S (ASTM D-1552 standard method) content determination. Proximate analysis was determined using a Mettler-Toledo TGA-DSC-1 thermogravimetric analyzer (TGA) by heating 3-5 mg samples in 70 μL alumina crucibles. Residual moisture in the pre-dried biomass (approximately 2-3% by mass) was removed from samples by heating to 110°C and holding for 15 minutes under a flow of 100 mL/min high purity nitrogen to obtain the dry sample mass. The volatile matter content was considered to be the mass loss between 110°C and 850 °C in nitrogen after a 30-minute hold, and the fixed carbon content the additional mass loss in 100 mL/min of dry air at 850 °C after 30 minutes. Residual inorganic matter, loosely termed "ash", was considered to be anything remaining after oxidation.

2.2 Silver Impregnation

An incipient wetness impregnation technique was used to incorporate silver into the biomass, whereby the BSG was soaked in a 0.1 M aqueous silver nitrate ($AgNO_3$) solution (ACROS Organics, 99.5% pure) in a ratio of 6 g biomass per 30 mL solution at room temperature and pressure. The soaked biomass sample was then vacuum filtered to remove excess solution and dried in a desiccator overnight. To understand the kinetics associated with silver metal loading onto our biomass, BSG samples were soaked in the silver nitrate solution for 2, 5, 10, 30, 60 minutes, and 24 hours in both 0.1 M aqueous silver nitrate and in de-ionized water as a control.

2.3 Thermal Treatment

Bio-templated materials are commonly produced by calcining metal-impregnated cellulosic samples around 450-500°C in air to remove the biomass template[81]. Production of materials in this manner does not allow for collection of biofuel given that the combustible products quickly oxidize upon devolatilization from the biomass. The novelty of the integrated biorefinery process is the ability to first collect biofuel products produced by pyrolysis prior to a calcination step. Thermal treatment of biomass samples was carried out using a 2-inch MTI tube furnace and porcelain boat containing samples (0.50 g of biomass). Based on derivative thermogravimetric (DTG) analysis, 500 °C was selected as the pyrolysis temperature, as more than 90% of mass loss occurs below this temperature and it is above the decomposition point of silver nitrate (440°C) and well below the melting point of silver (960°C). Under a 100 mL/min flow of high-purity nitrogen, samples were dried at 110°C for 15 minutes then heated to 500°C at a rate of 10°C/min and held at that temperature for 1 hour to ensure complete devolatilization. During pyrolysis, evolved gas was tracked with an Extorr RGA XT300M Quadrupole Mass Spectrometer starting at 110°C. Specifically, the m/z signals 2, 16, 26, 27, 30, and 44 were recorded (corresponding to H_2, CH_4, C_2H_2, C_2H_4, C_2H_6, and CO_2, respectively)[82,83]. CO evolution could not be monitored due to the fact that its primary m/z signal is 28, the same as N_2. In addition to monitoring pyrolysis gases, condensable vapors were collected in a 50 mL dichloromethane cold trap for later analysis. Upon completion of pyrolysis, the sample was exposed to 100 mL/min of dry air at 500°C for 1 hour to remove remaining organic material via oxidation. The sample was then allowed to cool to room temperature before being removed from the furnace. All pyrolysis experiments were repeated twice to ensure reproducibility of results.

2.4 Bio-Oil Analysis

Condensable bio-oil was collected in dichloromethane and analyzed using an Agilent 7890B gas chromatograph - 5977A MSD mass spectrometer (GC-MS). The analysis was performed in split-mode at a split ratio of 0.5 with Helium as the carrier gas. The GC injection temperature was 250°C. The GC oven was initially held for 10 minutes at 30°C then heated to 250°C at a rate of 3.35°C/min, and finally held at 250°C for 5 minutes. Interface temperature was set to 325°C. Mass spectra were recorded under electron ionization mode between m/z ratios of 29–300 after a 7-minute solvent delay. Integration of the largest GC peaks (by area) provided a means for semi-

quantitative analysis of the bio-oil compounds. Quantitative yield was calculated for select compounds for which a calibration curve was generated. Calibrated compounds were obtained from Fisher Scientific and ACROS Organics at minimum purities of 99.5 %; calibration curves had a minimum of 7 points spanning a concentration range of 10-700 ppm with minimum R^2 values of 0.994 as discussed in prior work[27,84]. A threshold of 90% match against the NIST compound library was used in identification of compounds, and validated against commonly detected biofuel components in the literature.

2.5 Thermal Analysis

Samples of raw and silver-impregnated biomass were placed into a 70 μL alumina crucible then inserted into a Mettler-Toledo TGA-DSC-1 for thermogravimetric analysis (TGA). The Distributed Activation Energy Model (DAEM) was applied to determine activation energy of pyrolysis[85]. All thermogravimetric experiments were completed in triplicate to ensure consistency of data and were performed in accordance with ICTAC Kinetics Committee suggestions to remove heating rate and transport dependencies on activation energy across one order of magnitude heating rates with small sample sizes, as used here[86]. Details of the DAEM are given in the online Supplemental Information (SI). To gauge overall reactivity of the sample, TGA plots of conversion, X(t), vs temperature of the solid were constructed using:

$$X(t) = \frac{m_0 - m_t}{m_0 - m_f} \quad (1)$$

where X(t) is the ratio of the mass of volatiles produced at a given time to the total mass at the end of the pyrolysis reaction, with initial mass as m_0, mass at time t as m_t, and m_f as mass after complete pyrolysis. Derivative thermogravimetric plots were constructed as dX(t)/dT(t) to show the dependence of reaction rate on temperature (which is a function of heating rate).

2.6 Biotemplated Silver Material Characterization

The presence and form of crystalline silver in the calcined sample was confirmed by X-ray Diffractometry (XRD) using a Bruker Discovery D-8 with Cu Kα radiation in the 2θ range of 30° to 90° at a 0.05° step with a sampling time of 0.5 seconds using a slit detector. Further characterization of the silver particles was performed by Scanning Electron Microscopy (SEM) analysis using a Zeiss Supra 55VP field emission scanning electron microscope. Calcined silver-impregnated samples were mounted on adhesive copper tape, gold coated, and imaged using the

SE2 detector at 2 kV. Energy Dispersive X-ray Spectrometry (EDS) analysis was also performed using an Apollo-40 EDAX detector at 7kV for samples on the same copper adhesive mounts.

3. Results and Discussion

To demonstrate the effectiveness of simultaneously bio-templating silver materials and *in situ* upgrading pyrolysis biofuels, we impregnated brewer's spent grain with silver nitrate prior to thermal treatment. Results of the proximate and ultimate analyses of the BSG are detailed in Table 1. After silver incorporation, the brewer's spent grain took on a noticeably darker color, presumably due to partial oxidation of the silver (images available in Figure S1 of online Supplemental Information, SI).

3.1 Optimal Soak Time

The silver nitrate solution soak time was considered in this analysis on the basis of practicality for scale-up, given that longer residence times for mixing may be associated with higher process costs. At scale, we envision silver incorporation into the biomass would take place while BSG is still wet, eliminating the pre-drying step. Figure 1 shows that the inorganic content of both the silver nitrate-soaked and water-soaked samples effectively did not change across this entire range of soak times (within a 95% confidence interval), nor did volatile or fixed carbon fractions within experimental error (data available in Figure S2 of SI). The data suggest that the kinetics of silver-to-biomass surface association are rapid, and a soak time on the order of minutes is sufficient for impregnation. Based on this analysis, all further BSG impregnation used a 2-minute silver nitrate soak time. Though some have suggested that a water pre-soak may serve to remove inorganic impurities present in biomass which might contaminate the nanomaterials[27,87–89], this effect is not observed for the water-soaked control; the as-received dried BSG and water-soaked BSG have identical proximate analyses within one standard deviation. This suggests that if purer bio-templated materials are desired, further pretreatment may be required such as by chelation. While this is the result for our BSG, it should be noted that this particular biomass feedstock has been extensively soaked in water throughout the brewing process.

3.2 Thermochemical Conversion of Raw and Silver-Impregnated Biomass

The impregnated biomass was pyrolyzed in a fixed bed reactor with approximately 0.5 g and the condensable and non-condensable biofuels analyzed via GC-MS and MS, respectively. After

completion of pyrolysis, the samples were calcined (oxidized) to remove remaining organic material and isolate the silver bio-templated materials. Table 2 shows the product distribution of solid, liquid and gas phases. The pyrolyzed fraction for the Ag-soaked biomass increases slightly; this becomes both the condensable and non-condensable portions, whereas the oxidized portion naturally decreases as silver is not lost, but remains in the biomass matrix

3.2.1 Analysis of Pyrolysis Gas

The gas evolution profile for the water-soaked BSG sample was virtually indistinguishable from the raw BSG. However, pyrolysis of the silver-impregnated BSG resulted in increased quantities of pyrolysis gas components evolved as compared to the raw, untreated biomass. The silver-impregnated sample evolved substantially more gas and at lower temperatures than the raw biomass, suggesting that the inclusion of silver into the biomass may serve to catalyze devolatilization (primary pyrolysis) of the biomass sample itself. A semi-quantitative comparison between treated and raw biomass can be made by integrating the area under the spectra (in partial pressures) for each gas component devolatilized during the pyrolysis residence time (Table 3). While evolution of CH_4, C_2H_2, and C_2H_4 were largely unaffected by the presence of the silver, hydrogen (H_2) and ethane (C_2H_6) evolution increased significantly (944% and 64%, respectively) in the silver-treated sample as shown in Figure 2 (figures for all gases monitored available in SI). The incorporated silver particles appear to enhance pyrolysis reactions as seen by distinct shifts in both noncondensable gases. This is particularly apparent in ethane evolution, which reaches peak evolution between 350 to 400°C with silver treatment, compared to at the maximum pyrolysis temperature of 500°C with raw BSG. Moreover, the profile of ethane production differed dramatically; the treated sample showed peaks at 340°C, 395°C, and 500°C, compared to a small peak at 320°C and a larger peak at 500°C in the raw sample. This result is also consistent—although the increase more dramatic—with those results observed by Xue *et al.* A 136% and 45% increase in devolatilization for hydrogen and ethane, respectively, was seen during pyrolysis of silver-treated corn stover, as well as 193% and 44%, respectively for silver-treated pure cellulose filter paper[27]. CO_2 evolution from Ag-treated BSG also increased 22%, similar to our prior work.

The effects on pyrolysis gas evolution observed here also agree with results from metal-catalyzed pyrolysis reported elsewhere in literature. Crystalline cellulose impregnated with both nickel

nitrate and iron nitrate yielded an increase in hydrogen and carbon dioxide, coupled with a decrease in CO and increase in H_2O and char formation[90]. $Ni(NO_3)_2$ impregnated wood shows increased generation of H_2 and CO while decreasing evolution of CO_2 and C-1 and C-2 hydrocarbons[91]. As previously noted, a catalyst's ability to devolatilize oxygen in the solid biomass matrix (e.g. as CO, CO_2, and H_2O) to reduce the oxygen content of the liquid fuel is an important consideration for improving the overall quality and stability of bio-oil. As Richardson *et al.* propose, water-gas shift reactions at the surface of impregnated Nickel nanoparticles may encourage the conversion carbon monoxide produced during pyrolysis to CO_2 and H_2 via oxidation by water[91]. Likewise, the oxidation of furfurals is also known to occur over heterogeneous catalysts which can shift the production of key intermediaries like 5-hydroxymethyl furfural to furan-based carboxylic acids[92]. Given that dismutation of CO to C and CO_2 by nano-Ni has also been observed[93], it is plausible that incorporated silver particles catalyze similar reactions, increasing carbon dioxide evolution, and possibly CO production (though this species was not measured in this study due to it sharing the same m/z signal as N_2). Further inquiry into the catalytic effects of silver on the bio-fuel products can be investigated by examination of the condensable bio-oil produced during pyrolysis.

3.2.2 Analysis of Bio-oil Components

Table 4 shows the bio-oil compounds identified by GC-MS analysis of the condensable bio-oil components collected in DCM during pyrolysis (full chromatograms in SI). The bio-oil formed from BSG pyrolysis is quite heterogeneous; BSG contains a complex mixture of cellulose, hemicellulose, lignin, carbohydrates, and proteins. However, it is reproducible and consistent for both "Raw" (as-received, dried) BSG and water-soaked BSG. As the GC-MS chromatograms show, the bio-oil originating from both raw and water-soaked BSG are almost identical (all the same peaks/compounds were detected; all but two compounds having areas within 2% of each other, one within 5%, one with 8%). Given this, we continue our comparative analysis of the catalytic impact of $AgNO_3$ impregnation as compared to Raw BSG.

As expected, the primary condensable components identified with a 90% or better NIST library match were furans, phenols, and alkanes with methyl and carbonyl substituent groups. Similar to prior studies on pyrolysis bio-oil from BSG, the primary compounds noted were holocellulose-derived, rather than lignin-derived compounds like phenols and benzenes[94]. Note that the

compounds listed in Table 3 represent only a portion of the total chromatogram area, and their relative areas are given as a fraction of the sum of top 20 GC peak areas. Although this analysis is semi-quantitative, it is nonetheless effective in demonstrating the effects of *in situ* fuel upgrading though incorporation of silver into the biomass feedstock. Quantitative yields of furfural, maple lactone, p-cresol, and phenol were calculated using GC-MS calibration curves. From this calibration data, we estimate that the condensable component yield (which includes condensed water) shows a slightly higher mass yield for raw BSG than $AgNO_3$-soaked BSG, as shown in Table 2. We note that the sample size was too small to measure water and acid content, but future work will explore this.

There are a multitude of reactions which the incorporated silver may encourage, including cracking, cyclization, hydrogenation, and dehydrogenation[95–98]. The underlying mechanism for many of these reactions is the ability of transition and noble metals to adsorb alkene, isocyanide, and aromatic compounds onto their surface due to interactions between the organic compounds' filled π-orbitals and the unoccupied d-orbitals of the metal, a phenomenon known as π back-bonding. The GC results for condensable bio-oil of the silver-treated sample show a slight increase in the quantity of compounds detected at longer retention times; however, the total GC peak areas were approximately unchanged from the untreated sample (full GC data available in SI). This, taken with increased gas devolatilization in the treated sample, suggests molecular rearrangement and dehydrogenation pathways may be preferred over a complete thermochemical cracking of the bio-oil fraction. However, while the chromatogram areas were not substantially changed, the yield of polycyclic aromatic hydrocarbons, comprising the vast majority of tars, were significantly lower. Anthracene and pyrene were detected in the raw sample at a yield of 6.2 and 1.3 g/kg_{BSG}, respectively, while only fluorene was detected in the silver impregnated sample with a yield of 0.19 g/kg_{BSG}.

Notably in this analysis, it was found that the silver-treated sample showed a marked increase in furfural, an important precursor in many chemical processes[99]. This agrees with reported observations of increased furans in bio-oil resulting from catalytic activity by silver, iron, and nickel species[100]. As Patwardhan, Satrio, and Brown propose, an increase in furan compounds may be due to these metals' ability to hemolytically and heterocyclically cleave pyranose rings and

glycosidic bonds[98]. In addition, a decrease in 2-methyl-propanal and 2-methyl-butanal was observed in the silver treated sample. It is possible that this, taken with the increased hydrogen gas evolution and furan yield, can be attributed to a dehydrogenation process via cyclization of linear aldehyde compounds at the silver surface. Prior literature notes that furan ring derivatives may be formed from cyclization followed by dehydration of C4, C5 and C6 fragments generated from pyrolysis[101].

Catalytic biomass pyrolysis by zeolites and other solid acid catalysts are known to encourage dehydration and decarbonylation/decarboxylation reactions (breaking of C-OH and C-CO(OH) bonds)[102]. Additionally, silver nitrate has been previously shown to catalyze decarboxylation of saturated and unsaturated fatty acids, silver (I) to decarboxylate aryl carboxylates, and silver (II) to decarboxylate certain amino acids[103]. Given the increase in CO_2 gas evolved after silver treatment, with the decrease in phenol yield and increase in furfural in the bio-oil fraction, it is possible that the silver promotes decarboxylation reactions during pyrolysis. Similarly, increased devolatilization of hydrogen gas may indicate that silver is catalyzing dehydration reactions, perhaps favoring H_2 formation over H_2O given BSG's lower oxygen content (36% versus 40 and 49% in feed corn and raw cellulose, respectively)[104].

3.2.3 Thermochemical Conversion Kinetics

A chemical catalyst should lower activation energy (E_a) of pyrolysis and/or increase pyrolytic reaction rates. Table 5 shows peak DTG conversion rates and temperatures for the four experimental heating rates. As seen in the sample DTG plot of Figure 3 (all plots available in SI), there are multiple peaks for each biomass sample. Peak 1, which only appears in the raw BSG, is likely attributable to "brewing residue" comprised of soluble proteins and yeast coating the dried brewer's spent grain following fermentation. (In all experiments, soaking the BSG produced a yellow-colored raffinate). All samples show Peak 2 and Peak 3; these peaks are roughly attributed to the breakdown and subsequent devolatilization of hemicellulose and cellulose, respectively. Although not observed to be as prominent as hemicellulose and cellulose decomposition here; thermal breakdown of lignin is known to occur at temperatures roughly above 450 °C.[105] The peak pyrolytic reactivity temperature of roughly 280-340 °C, as determined by DTG at 10 °C/min,

aligns with devolatilization patterns observed in bulk pyrolysis for CO_2, CH_4, and C_2H_6 release. Other gasses recorded did not begin to devolatilize significantly until 400-500 °C.

For the range of heating rates, the silver-treated BSG shows a consistent trend towards lower peak reaction temperature for both hemicellulose and cellulose decomposition, while the opposite trend is seen for water-only soaked samples. Across the range of heating rates, peak hemicellulose (Peak 2) reactivity for Ag-BSG was shifted lower by 0 to 7°C versus raw BSG, and 9—15°C lower than water-soaked BSG. Peak cellulose (Peak 3) reactivity for Ag-BSG occurred 4—11°C lower than raw BSG and 11—28°C lower than the water-soaked BSG. Along with peak shifting, the leading and trailing edges of the DTG curve for Ag-BSG were also noticeably shifted towards lower temperatures as compared to water-soaked BSG. This agrees with gas evolution temperature profiles, which show increased reactivity at lower temperature ranges for silver-treated samples. Though peak reactivity temperatures are lower, peak reaction *rates* for cellulose and hemicellulose decomposition in the silver-treated and raw BSG show little difference, with the Ag-BSG samples displaying slightly lower reaction rates at higher heating rates. For the water-soaked sample the peak reactivity was 31-39% higher for hemicellulose decomposition as compared to the raw, un-soaked sample (though only 2-7% higher for cellulose decomposition). This increase is not observed for the aqueous silver nitrate soaked samples. This is possibly attributable to the more amorphous structure of hemicellulose, which is more prone to hydrolysis by dilute acids or bases, and interactions with certain ionic compounds in the soaked solution[106]. The apparent suppression of hemicellulose decomposition in the silver-soaked sample may therefore be due to effects of the nitrate anion, e.g. as a buffer within the raffinate, during the soaking step.

The activation energy as a function of mass fractional conversion (Figure 4a) shows $E_a(X)$ for silver-treated BSG is slightly higher than that of raw BSG across the entire conversion range, though often within a 95% confidence interval. $E_a(X)$ for the soaked and un-soaked raw BSG samples are similar, though E_a of the soaked sample is higher and statistically significant below X=0.4. Again, this may be explained by residual brewing residue being washed away. Figure 4b, shows the overall average activation energies of pyrolysis for the samples: 160±29 kJ/mol, 179±21 kJ/mol, 166±13 kJ/mol for raw, Ag-treated, and water-soaked BSG, respectively. The confidence intervals given here represent standard deviation of average conversion values — note, the

variance in activation energies at the various conversion levels leads to a fairly large standard deviation.

Although the incorporation of silver does not directly increase the peak pyrolytic reaction rate in BSG (as determined by DTG), nor lower the overall pyrolytic activation energy barrier, it does lead to increased yield of bio-gas components and alters the yield of bio-oil marker compounds without changing E_a significantly, as well as lowering peak reactivity temperatures. As literature reveals, it is not uncommon to observe increased pyrolysis gas evolution without a corresponding drop in activation energy during *in-situ* biofuel upgrading[107]. While incorporation of metals or metal oxides may or may not lower the overall activation energy barrier for biomass pyrolysis, there are certain reactions or groups of reactions which are encouraged more so than others by their inclusion, signifying catalytic behavior[108]. In fact, activation energy effects have been demonstrated to be feedstock-specific even for the same catalyst material[109,110]. Thus, the practicality of a pyrolysis catalyst should be evaluated holistically based on a combination of changes to bio-gas and bio-oil components, yield, and overall activation energy across the thermochemical conversion range.

3.3 Bio-templated Silver Particles

The yield of silver, post-calcination, is approximately 5.59 g/kg_{BSG} (of raw biomass). This silver loading is comparable to the observed yields for prior work[27] on corn stover and cellulose paper samples treated with 0.1 M $AgNO_3$. The XRD spectrum of the calcined silver-impregnated biomass (SI) confirms the signature peaks for face-centered cubic (fcc) crystalline elemental silver at 2θ angles of 38.0°, 44.1°, 64.3°, 77.3°, and 81.4°, corresponding to d-spacings of (111), (200), (220), (311), and (222), respectively[111]. Additionally, SEM images of the calcined silver-impregnated biomass (Figure 5) clearly show a number of faceted structures not present in the untreated samples, presumably our bio-templated silver. The metal particles formed from the BSG scaffold in this work are similar to other heterogeneous biomass templates, which appear to produce a wider size distribution with larger average particle sizes as compared to plant extracts or pure cellulose[112,113]. Both He *et al.* and Xue *et al.* have observed bio-templated silver particle size and morphology to be a strong function of the biomass feedstock, ranging in diameter from 5 nm to several hundred nanometers and from semi-spherical mesh to well-formed individual particles[27,81].

The practicality of bio-templating nanoparticles using heterogeneous feedstocks will depend, along with particle size distribution, on the requisite purity of nanomaterials; additional biomass pretreatment may be necessary to improve these characteristics for certain applications. Through EDS, the presence of silver on our calcined samples was also confirmed, and the support material seen in the SEM images was determined primarily to be carbonaceous char. Further analysis of the bulk carbonaceous support showed traces of Mg, Si, P, K, and Ca—inorganic compounds likely taken up by the grains from the soil in which brewers' grain is grown. Thus, it is possible that the silver particles contain some fraction of these contaminants, albeit in amorphous form since XRD did not detect other crystalline forms.

Separation of these silver materials from the carbonaceous char support is another important practical consideration, since as seen here, the carbonaceous support may not fully oxidize away at temperatures lower than 500°C. A higher calcination temperature could be investigated provided there was no degradation to the particles[114], although this (1) risks approaching the melting point of silver and particles fusing and (2) would require Ag-ash separation would nonetheless be required. From an overall process perspective, it could be more advantageous to explore the utility of metal-impregnated bio-char materials. In fact, a substantial body of literature exists surrounding the functionalization of bio-char for catalysis and adsorption since bio-char alone has fairly poor surface functionality, somewhat limiting its material applications[115–117]. Such heterogeneous biochar-catalyst composites are emerging as catalysts for downstream biorefinery applications[118]. Numerous examples of metal-impregnated biochar have been explored for applications ranging from water treatment to selective separation processes[119,120]. A silver-impregnated biochar material might also find use in medical applications given the antimicrobial/antiviral/antifungal properties of nano-silver[121], combined with the high adsorption capacity of activated carbon[122]. Zhou *et al.* demonstrated iron-impregnated biochar's ability to sorb and reduce Ag^{+} ions from aqueous solution resulting in a material with strong antimicrobial activity[123]. Depending on the desired application, future work may consider the effect of altering process variables (e.g. biomass feedstock, soak time, silver nitrate concentration, biomass particle size) on silver-biomass loading, silver particle morphology, particle size distribution, and purity.

4. Conclusions

This work proposes an integrated bio-refinery model wherein upgraded biofuels and inorganic bio-templated materials can be co-produced during pyrolysis. Impregnation of brewer's spent grain with silver nitrate followed by slow pyrolysis showed a nearly 10-fold increase in hydrogen gas evolution at the same temperature, along with a 64% increase in ethane generation. In addition, increased devolatilization of CO_2 suggests oxygen elimination from the solid biomass matrix, and therefore from the resultant liquid fuel product. Condensable pyrolysis bio-oil from the Ag-impregnated samples showed significantly higher furfural yield with a corresponding decrease in C3-C4 linear aldehydes and phenol, suggesting dehydrogenation, cyclization, and decarboxylation may be among the reactions selectively encouraged by incorporating silver into the biomass matrix. Silver nitrate treatment did not statistically impact the average activation energy of pyrolysis. Although the overall activation energy barrier did not decrease with silver impregnation, the effects on pyrolysis gas and bio-fuel products strongly suggests a chemically catalytic activity. Silver micro- and nano-particles can be formed using a biomass scaffold and thus produce silver-impregnated char material as a value-added product of bio-fuel upgrading.

Acknowledgements

The authors appreciate the assistance of Luca Fiori and Maurizio Volpe in performing the Ultimate Analysis, support from the Boston University Initiative on Cities, the U.S.—Italy Fulbright Commission and the China Scholarship Council. A portion of this work was supported by the National Science Foundation under grant number 1933071 "Collaborative Research: Integrated Biorefinery for Pyrolysis Biofuels and Biotemplated Nanomaterials."

References

(1) Koonin, S. E. Getting Serious about Biofuels. *Science*. 2006, p 435. https://doi.org/10.1126/science.1124886.

(2) Williams, C. C. K.; Templer, R.; Murphy, R.; Leak, D. D. J.; Ragauskas, A. A. J.; Williams, C. C. K.; Davison, B. B. H.; Britovsek, G.; Cairney, J.; Eckert, C. A.; et al. The Path Forward for Biofuels and Biomaterials. *Science (80-.).* **2006**, *311* (5760).

(3) Cherubini, F. The Biorefinery Concept: Using Biomass Instead of Oil for Producing Energy and Chemicals. *Energy Convers. Manag.* **2010**, *51* (7), 1412–1421.

(4) Corma Canos, A.; Iborra, S.; Velty, A. Chemical Routes for the Transformation of Biomass into Chemicals. *Chemical Reviews*. 2007, pp 2411–2502. https://doi.org/10.1021/cr050989d.

(5) Gallezot, P. Catalytic Routes from Renewables to Fine Chemicals. *Catal. today* **2007**.

(6) Shuttleworth, P. S.; De bruyn, M.; Parker, H. L.; Hunt, a. J.; Budarin, V. L.; Matharu, a. S.; Clark, J. H. Applications of Nanoparticles in Biomass Conversion to Chemicals and Fuels. *Green Chem.* **2014**, *16* (2), 573. https://doi.org/10.1039/c3gc41555d.

(7) Zhang, Q.; Chang, J.; Wang, T.; Xu, Y. Review of Biomass Pyrolysis Oil Properties and Upgrading Research. *Energy Convers. Manag.* **2007**, *48* (1), 87–92. https://doi.org/10.1016/j.enconman.2006.05.010.
(8) Iisa, K.; Robichaud, D. J.; Watson, M. J.; ten Dam, J.; Dutta, A.; Mukarakate, C.; Kim, S.; Nimlos, M. R.; Baldwin, R. M. Improving Biomass Pyrolysis Economics by Integrating Vapor and Liquid Phase Upgrading. *Green Chem.* **2018**, *20* (3), 567–582. https://doi.org/10.1039/C7GC02947K.
(9) Chacón-Huete, F.; Messina, C.; Chen, F.; Cuccia, L.; Ottenwaelder, X.; Forgione, P. Solvent-Free Mechanochemical Oxidation and Reduction of Biomass-Derived 5-Hydroxymethyl Furfural. *Green Chem.* **2018**. https://doi.org/10.1039/c8gc02481b.
(10) Zhang, S.; Yan, Y.; Li, T.; Ren, Z. Upgrading of Liquid Fuel from the Pyrolysis of Biomass. *Bioresour. Technol.* **2005**, *96* (5), 545–550.
(11) Pinho, A. de R.; Almeida, M. de. Co-Processing Raw Bio-Oil and Gasoil in an FCC Unit. *Fuel Process.* **2015**.
(12) Wang, L.; Xiao, F.-S. Nanoporous Catalysts for Biomass Conversion. *Green Chem.* **2015**, *17* (1), 24–39. https://doi.org/10.1039/C4GC01622J.
(13) Xiu, S.; Shahbazi, A. Bio-Oil Production and Upgrading Research: A Review. *Renew. Sustain. Energy Rev.* **2012**, *16* (7), 4406–4414.
(14) Poonjarernsilp, C.; Sano, N.; Sawangpanich, N. Effect of Fe/Fe 2 O 3 Loading on the Catalytic Activity of Sulfonated Single-Walled Carbon Nanohorns for the Esterification of Palmitic Acid. *Green Chem.* **2014**, *16* (12), 4936–4943.
(15) Wu, H.; Zhang, J.; Wei, Q.; Zheng, J.; Zhang, J. Transesterification of Soybean Oil to Biodiesel Using Zeolite Supported CaO as Strong Base Catalysts. *Fuel Process. Technol.* **2013**, *109* (2), 13–18. https://doi.org/10.1016/j.fuproc.2012.09.032.
(16) Geboers, J.; Vyver, S. Van de; Carpentier, K. Efficient Catalytic Conversion of Concentrated Cellulose Feeds to Hexitols with Heteropoly Acids and Ru on Carbon. *Chem. Commun.* **2010**, *46* (20), 3577–3579.
(17) Deng, W.; Tan, X.; Fang, W.; Zhang, Q.; Wang, Y. Conversion of Cellulose into Sorbitol over Carbon Nanotube-Supported Ruthenium Catalyst. *Catal. Letters* **2009**, *133* (1–2), 167–174. https://doi.org/10.1007/s10562-009-0136-3.
(18) Wang, A.; Zhang, T. One-Pot Conversion of Cellulose to Ethylene Glycol with Multifunctional Tungsten-Based Catalysts. *Acc. Chem. Res.* **2013**, *46* (7), 1377–1386.
(19) Liang, G.; Wu, C.; He, L.; Ming, J.; Cheng, H.; Zhuo, L. Selective Conversion of Concentrated Microcrystalline Cellulose to Isosorbide over Ru/C Catalyst. *Green* **2011**.
(20) Op De Beeck, B.; Geboers, J.; Van De Vyver, S.; Van Lishout, J.; Snelders, J.; Huijgen, W. J. J.; Courtin, C. M.; Jacobs, P. A.; Sels, B. F. Conversion of (Ligno)Cellulose Feeds to Isosorbide with Heteropoly Acids and Ru on Carbon. *ChemSusChem* **2013**, *6* (1), 199–208. https://doi.org/10.1002/cssc.201200610.
(21) Torri, C.; Lesci, I.; Fabbri, D. Analytical Study on the Pyrolytic Behaviour of Cellulose in the Presence of MCM-41 Mesoporous Materials. *J. Anal. Appl. Pyrolysis* **2009**, *85* (1), 192–196.
(22) Fabbri, D.; Torri, C.; Baravelli, V. Effect of Zeolites and Nanopowder Metal Oxides on the Distribution of Chiral Anhydrosugars Evolved from Pyrolysis of Cellulose: An Analytical Study. *J. Anal. Appl. Pyrolysis* **2007**, *80* (1), 24–29.
(23) Lu, Q.; Xiong, W. M.; Li, W. Z.; Guo, Q. X.; Zhu, X. F. Catalytic Pyrolysis of Cellulose with Sulfated Metal Oxides: A Promising Method for Obtaining High Yield of Light

570 Furan Compounds. *Bioresour. Technol.* **2009**, *100* (20), 4871–4876.
571 https://doi.org/10.1016/j.biortech.2009.04.068.
572 (24) Gökdai, Z.; Sınağ, A.; Yumak, T. Comparison of the Catalytic Efficiency of Synthesized
573 Nano Tin Oxide Particles and Various Catalysts for the Pyrolysis of Hazelnut Shell.
574 *Biomass and Bioenergy* **2010**, *34* (3), 402–410.
575 (25) Kastner, J.; Hilten, R.; Weber, J.; McFarlane, A. Continuous Catalytic Upgrading of Fast
576 Pyrolysis Oil Using Iron Oxides in Red Mud. *RSC Adv.* **2015**, *5* (37), 29375–29385.
577 (26) Ben, H.; Huang, F.; Li, L.; Ragauskas, A. In Situ Upgrading of Whole Biomass to Biofuel
578 Precursors with Low Average Molecular Weight and Acidity by the Use of Zeolite
579 Mixture. *RSC Adv.* **2015**, *5* (91), 74821–74827.
580 (27) Xue, J.; Dou, G.; Ziade, E.; Goldfarb, J. L. Integrating Sustainable Biofuel and Silver
581 Nanomaterial Production for in Situ Upgrading of Cellulosic Biomass Pyrolysis. *Energy*
582 *Convers. Manag.* **2017**, *142*, 143–152. https://doi.org/10.1016/j.enconman.2017.03.001.
583 (28) Elliott, D. C. Catalytic Hydrothermal Gasification of Biomass. *Biofuels, Bioproducts and*
584 *Biorefining*. John Wiley & Sons, Ltd May 1, 2008, pp 254–265.
585 https://doi.org/10.1002/bbb.74.
586 (29) Falsig, H.; Hvolbæk, B.; Kristensen, I. S.; Jiang, T.; Bligaard, T.; Christensen, C. H.;
587 Nørskov, J. K. Trends in the Catalytic CO Oxidation Activity of Nanoparticles. *Angew.*
588 *Chemie* **2008**, *120* (26), 4913–4917. https://doi.org/10.1002/ange.200801479.
589 (30) Shen, Y.; Yoshikawa, K. Recent Progresses in Catalytic Tar Elimination during Biomass
590 Gasification or Pyrolysis - A Review. *Renewable and Sustainable Energy Reviews*. 2013,
591 pp 371–392. https://doi.org/10.1016/j.rser.2012.12.062.
592 (31) Studt, F.; Abild-Pedersen, F.; Wu, Q.; Jensen, A. D.; Temel, B.; Grunwaldt, J. D.;
593 Norskov, J. K. CO Hydrogenation to Methanol on Cu-Ni Catalysts: Theory and
594 Experiment. *J. Catal.* **2012**, *293*, 51–60. https://doi.org/10.1016/j.jcat.2012.06.004.
595 (32) Wang, S.; Temel, B.; Shen, J.; Jones, G.; Grabow, L. C.; Studt, F.; Bligaard, T.; Abild-
596 Pedersen, F.; Christensen, C. H.; Nørskov, J. K. Universal Br??Nsted-Evans-Polanyi
597 Relations for C-C, C-O, C-N, N-O, N-N, and O-O Dissociation Reactions. *Catal. Letters*
598 **2011**, *141* (3), 370–373. https://doi.org/10.1007/s10562-010-0477-y.
599 (33) InfoMine Inc. Commodity and Metal Prices http://www.infomine.com/investment/metal-
600 prices/ (accessed Jan 20, 2019).
601 (34) Zargar, M.; Hamid, A. A.; Bakar, F. A.; Shamsudin, M. N.; Shameli, K.; Jahanshiri, F.;
602 Farahani, F. Green Synthesis and Antibacterial Effect of Silver Nanoparticles Using Vitex
603 Negundo L. *Molecules* **2011**, *16* (8), 6667–6676.
604 https://doi.org/10.3390/molecules16086667.
605 (35) Rujitanaroj, P.; Pimpha, N.; Supaphol, P. Wound-Dressing Materials with Antibacterial
606 Activity from Electrospun Gelatin Fiber Mats Containing Silver Nanoparticles. *Polymer*
607 *(Guildf).* **2008**.
608 (36) Tulve, N. S.; Stefaniak, A. B.; Vance, M. E.; Rogers, K.; Mwilu, S.; LeBouf, R. F.;
609 Schwegler-Berry, D.; Willis, R.; Thomas, T. A.; Marr, L. C. Characterization of Silver
610 Nanoparticles in Selected Consumer Products and Its Relevance for Predicting Children's
611 Potential Exposures. *Int. J. Hyg. Environ. Health* **2015**, *218* (3), 345–357.
612 https://doi.org/10.1016/j.ijheh.2015.02.002.
613 (37) Fan, T. X. T.; Chow, S. K. S.; Zhang, D. *Biomorphic Mineralization: From Biology to*
614 *Materials*; 2009; Vol. 54, pp 542–659. https://doi.org/10.1016/j.pmatsci.2009.02.001.
615 (38) Huang, J.; Lin, L.; Sun, D.; Chen, H.; Yang, D.; Li, Q. Bio-Inspired Synthesis of Metal

Nanomaterials and Applications. *Chem. Soc. Rev.* **2015**, *44* (17), 6330–6374. https://doi.org/10.1039/C5CS00133A.
(39) Martin-Martinez, F. J.; Jin, K.; López Barreiro, D.; Buehler, M. J. The Rise of Hierarchical Nanostructured Materials from Renewable Sources: Learning from Nature. *ACS Nano* **2018**, acsnano.8b04379. https://doi.org/10.1021/acsnano.8b04379.
(40) Vilchis-Nestor, A.; Sánchez-Mendieta, V. Solventless Synthesis and Optical Properties of Au and Ag Nanoparticles Using Camellia Sinensis Extract. *Mater. Lett.* **2008**.
(41) Bao, S.-J.; Lei, C.; Xu, M.-W.; Cai, C.-J.; Cheng, C.-J.; Li, C. M. Environmentally-Friendly Biomimicking Synthesis of TiO2 Nanomaterials Using Saccharides to Tailor Morphology, Crystal Phase and Photocatalytic Activity. *CrystEngComm* **2013**, *15* (23), 4694. https://doi.org/10.1039/c3ce40310f.
(42) Varma, R. Journey on Greener Pathways: From the Use of Alternate Energy Inputs and Benign Reaction Media to Sustainable Applications of Nano-Catalysts in Synthesis. *Green Chem.* **2014**.
(43) Adlakha-Hutcheon, G.; Khaydarov, R.; Korenstein, R.; Varma, R.; Vaseashta, A.; Stamm, H.; Abdel-Mottaleb, M. Nanomaterials, Nanotechnology. In *Nanomaterials: Risks and Benefits*; Springer Netherlands: Dordrecht, 2009; pp 195–207. https://doi.org/10.1007/978-1-4020-9491-0_14.
(44) Rafael, L.; S, V. R.; Varma, R. S.; H, C. J.; Kraus, G. a. *Sustainable Preparation of Metal Nanoparticles: Methods and Applications*, 1st ed.; Luque, R., Varma, R. S., Eds.; The Royal Society of Chemistry: Cambridge, 2012. https://doi.org/10.1039/9781849735469.
(45) Vigneshwaran, N.; Nachane, R. A Novel One-Pot 'green'synthesis of Stable Silver Nanoparticles Using Soluble Starch. *Carbohydr. Res.* **2006**, *341* (12), 2012–2018.
(46) Bakar, N.; Ismail, J.; Bakar, M. Synthesis and Characterization of Silver Nanoparticles in Natural Rubber. *Mater. Chem. Phys.* **2007**.
(47) Ahmad, N.; Sharma, S. Green Synthesis of Silver Nanoparticles Using Extracts of Ananas Comosus. *Green Sustain. Chem.* **2012**, *2* (November), 141–147. https://doi.org/10.4236/gsc.2012.24020.
(48) Kouvaris, P.; Delimitis, A.; Zaspalis, V.; Papadopoulos, D.; Tsipas, S. A.; Michailidis, N. Green Synthesis and Characterization of Silver Nanoparticles Produced Using Arbutus Unedo Leaf Extract. *Mater. Lett.* **2012**, *76*, 18–20. https://doi.org/10.1016/j.matlet.2012.02.025.
(49) Ajitha, B.; Reddy, Y. A. K.; Reddy, P. S. Biosynthesis of Silver Nanoparticles Using Momordica Charantia Leaf Broth: Evaluation of Their Innate Antimicrobial and Catalytic Activities. *J. Photochem. Photobiol. B Biol.* **2015**, *146*, 1–9. https://doi.org/10.1016/j.jphotobiol.2015.02.017.
(50) He, J.; Kunitake, T.; Nakao, A. Facile In Situ Synthesis of Noble Metal Nanoparticles in Porous Cellulose Fibers. *Chem. Mater.* **2003**, *15* (23), 4401–4406. https://doi.org/10.1021/cm034720r.
(51) Cao, J.; Rusina, O.; Sieber, H. Processing of Porous TiO2-Ceramics from Biological Preforms. In *Ceramics International*; 2004; Vol. 30, pp 1971–1974. https://doi.org/10.1016/j.ceramint.2003.12.180.
(52) Chang, Y. C.; Lee, C. Y.; Chiu, H. T. Porous Inorganic Materials from Living Porogens: Channel-like TiO 2 from Yeast-Assisted Sol-Gel Process. *ACS Appl. Mater. Interfaces* **2014**, *6* (1), 31–35. https://doi.org/10.1021/am405149a.
(53) Venkataramanan, N. N. S.; Matsui, K.; Kawanami, H.; Ikushima, Y. Green Synthesis of

Titania Nanowire Composites on Natural Cellulose Fibers. *Green Chem.* **2007**, *9* (1), 18. https://doi.org/10.1039/b609887h.
(54) Cao, F.; Li, D. Biotemplate Synthesis of Monodispersed Iron Phosphate Hollow Microspheres. **2010**, *5* (5), 16005–16006. https://doi.org/10.1088/1748-3182/5/1/016005.
(55) Kim, Y. Small Structures Fabricated Using Ash-Forming Biological Materials as Templates. *Biomacromolecules* **2003**, *4* (4), 908–913. https://doi.org/10.1021/bm0257558.
(56) Zhou, W.; He, W.; Zhang, X.; Yan, S.; Sun, X.; Tian, X.; Han, X. Biosynthesis of Iron Phosphate Nanopowders. *Powder Technol.* **2009**, *194* (1–2), 106–108. https://doi.org/10.1016/j.powtec.2009.03.034.
(57) Dong, Q.; Su, H.; Xu, J.; Zhang, D.; Wang, R. Synthesis of Biomorphic ZnO Interwoven Microfibers Using Eggshell Membrane as the Biotemplate. *Mater. Lett.* **2007**. https://doi.org/10.1016/j.matlet.2006.06.091.
(58) Zhang, W.; Zhang, D.; Fan, T.; Ding, J.; Guo, Q.; Ogawa, H. Fabrication of ZnO Microtubes with Adjustable Nanopores on the Walls by the Templating of Butterfly Wing Scales. *Nanotechnology* **2006**, *17* (3), 840–844. https://doi.org/10.1088/0957-4484/17/3/038.
(59) Upneja, A.; Dou, G.; Gopu, C.; Johnson, C. A. C. A.; Newman, A.; Suleimenov, A.; Goldfarb, J. L. Sustainable Waste Mitigation: Biotemplated Nanostructured ZnO for Photocatalytic Water Treatment via Extraction of Biofuels from Hydrothermal Carbonization of Banana Stalk. *RSC Adv.* **2016**, *6* (95).
(60) Dallas, P.; Sharma, V.; Zboril, R. Silver Polymeric Nanocomposites as Advanced Antimicrobial Agents: Classification, Synthetic Paths, Applications, and Perspectives. *Adv. Colloid Interface Sci.* **2011**.
(61) Wang, F.; Hu, S. Electrochemical Sensors Based on Metal and Semiconductor Nanoparticles. *Microchim. Acta* **2009**.
(62) Mishra, P. K.; Gregor, T.; Wimmer, R. Utilising Brewer's Spent Grain as a Source of Cellulose Nanofibres Following Separation of Protein-Based Biomass. *BioResources* **2017**, *12* (1), 107–116. https://doi.org/10.15376/biores.12.1.107-116.
(63) Mussatto, S. I.; Dragone, G.; Roberto, I. C. Brewers' Spent Grain: Generation, Characteristics and Potential Applications. *Journal of Cereal Science*. Academic Press January 1, 2006, pp 1–14. https://doi.org/10.1016/j.jcs.2005.06.001.
(64) Santos, M.; Jiménez, J. .; Bartolomé, B.; Gómez-Cordovés, C.; del Nozal, M. . Variability of Brewer's Spent Grain within a Brewery. *Food Chem.* **2003**, *80* (1), 17–21. https://doi.org/10.1016/S0308-8146(02)00229-7.
(65) Ben-Hamed, U.; Seddighi, H.; Thomas, K. Economic Returns of Using Brewery's Spent Grain in Animal Feed. *Int. J. Econ. Manag. Eng.* **2011**, *5* (2), 142–145.
(66) Aliyu, S.; Bala, M. Brewer's Spent Grain: A Review of Its Potentials and Applications. *African J. Biotechnol.* **2011**, *10* (3), 324–331. https://doi.org/10.5897/AJBx10.006.
(67) Vanreppelen, K.; Vanderheyden, S.; Kuppens, T.; Schreurs, S.; Yperman, J.; Carleer, R. Activated Carbon from Pyrolysis of Brewer's Spent Grain: Production and Adsorption Properties. *Waste Manag. Res.* **2014**, *32* (7), 634–645. https://doi.org/10.1177/0734242X14538306.
(68) Cooray, S. T.; Chen, W. N. Valorization of Brewer's Spent Grain Using Fungi Solid-State Fermentation to Enhance Nutritional Value. *J. Funct. Foods* **2018**, *42*, 85–94. https://doi.org/10.1016/j.jff.2017.12.027.
(69) Okamoto, H.; Sato, K.; Yagi, N.; Inoue, M.; Yamasaki, S.; Ishida, S.; Shibata, J.

Development of Production Process of Charcoal Bricks from Spent Grain. *KAGAKU KOGAKU RONBUNSHU* **2002**, *28* (2), 137–142. https://doi.org/10.1252/kakoronbunshu.28.137.
(70) Sato, K.; Yagi, N.; Okamoto, H.; Inoue, M.; Ajiri, T.; Shibata, J. Physical Property and Burning Property of Spent Grain Charcoal. *Shigen-to-Sozai* **2001**, *117* (7), 587–590. https://doi.org/10.2473/shigentosozai.117.587.
(71) Xiros, C.; Christakopoulos, P. Enhanced Ethanol Production from Brewer's Spent Grain by a Fusarium Oxysporum Consolidated System. *Biotechnol. Biofuels* **2009**, *2* (1), 4. https://doi.org/10.1186/1754-6834-2-4.
(72) Xiros, C.; Topakas, E.; Katapodis, P.; Christakopoulos, P. Hydrolysis and Fermentation of Brewer's Spent Grain by Neurospora Crassa. *Bioresour. Technol.* **2008**, *99* (13), 5427–5435. https://doi.org/10.1016/j.biortech.2007.11.010.
(73) De Smidt, O.; Du Preez, J. C.; Albertyn, J. The Alcohol Dehydrogenases of Saccharomyces Cerevisiae: A Comprehensive Review. In *FEMS Yeast Research*; 2008; Vol. 8, pp 967–978. https://doi.org/10.1111/j.1567-1364.2008.00387.x.
(74) Ezeonu, F. C.; Okaka, A. N. C. Process Kinetics and Digestion Efficiency of Anaerobic Batch Fermentation of Brewer's Spent Grains (BSG). *Process Biochem.* **1996**, *31* (1), 7–12. https://doi.org/10.1016/0032-9592(94)00064-6.
(75) Sežun, M.; Grilc, V.; Zupančič, G. D.; Logar, R. M. Anaerobic Digestion of Brewery Spent Grain in a Semi-Continuous Bioreactor: Inhibition by Phenolic Degradation Products. *Acta Chim. Slov.* **2011**, *58* (1), 158–166. https://doi.org/10.15585/mmwr.mm6712a1.
(76) Bochmann, G.; Drosg, B.; Fuchs, W. Anaerobic Digestion of Thermal Pretreated Brewers' Spent Grains. *Environ. Prog. Sustain. Energy* **2015**, *34* (4), 1092–1096. https://doi.org/10.1002/ep.12110.
(77) Mahmood, A. S. N.; Brammer, J. G.; Hornung, A.; Steele, A.; Poulston, S. The Intermediate Pyrolysis and Catalytic Steam Reforming of Brewers Spent Grain. In *Journal of Analytical and Applied Pyrolysis*; Elsevier, 2013; Vol. 103, pp 328–342. https://doi.org/10.1016/j.jaap.2012.09.009.
(78) Goldfarb, J. L.; Ceylan, S. Second-Generation Sustainability: Application of the Distributed Activation Energy Model to the Pyrolysis of Locally Sourced Biomass-Coal Blends for Use in Co-Firing Scenarios. *Fuel* **2015**, *160*. https://doi.org/10.1016/j.fuel.2015.07.071.
(79) McGreevy, J. 2015-2016 Beer Institute Annual Report http://www.beerinstitute.org/wp-content/uploads/2016/11/BeerInstitute_AnnualReport_090316-pages.pdf (accessed Nov 17, 2018).
(80) Xue, J.; Chellappa, T.; Ceylan, S.; Goldfarb, J. L. Enhancing Biomass + Coal Co-Firing Scenarios via Biomass Torrefaction and Carbonization: Case Study of Avocado Pit Biomass and Illinois No. 6 Coal. *Renew. Energy* **2018**, *122*, 152–162. https://doi.org/10.1016/j.renene.2018.01.066.
(81) He, J.; Kunitake, T.; Watanabe, T. Porous and Nonporous Ag Nanostructures Fabricated Using Cellulose Fiber as a Template. *Chem Commun* **2005**, *1* (6), 795–796. https://doi.org/10.1039/b416316h.
(82) Evans, R.; Milne, T. Molecular Characterization of the Pyrolysis of Biomass. *Energy & Fuels* **1987**, *1* (2), 123–137.
(83) Huang, Y. F.; Kuan, W. H.; Chiueh, P. T.; Lo, S. L. Pyrolysis of Biomass by Thermal

754 Analysis – Mass Spectrometry (TA – MS). *Bioresour. Technol.* **2011**, *102*, 3527–3534.
755 https://doi.org/10.1016/j.biortech.2010.11.049.
756 (84) Dou, G.; Goldfarb, J. In Situ Upgrading of Pyrolysis Biofuels by Bentonite Clay with
757 Simultaneous Production of Heterogeneous Adsorbents for Water Treatment. *Fuel* **2017**,
758 *195*, 273–283. https://doi.org/10.1016/j.fuel.2017.01.052.
759 (85) Cai, J.; Liu, R. New Distributed Activation Energy Model: Numerical Solution and
760 Application to Pyrolysis Kinetics of Some Types of Biomass. *Bioresour Technol* **2008**, *99*
761 (8), 2795–2799. https://doi.org/10.1016/j.biortech.2007.06.033.
762 (86) Vyazovkin, S.; Chrissafis, K.; Di Lorenzo, M. L.; Koga, N.; Pijolat, M.; Roduit, B.;
763 Sbirrazzuoli, N.; Suñol, J. J. ICTAC Kinetics Committee Recommendations for Collecting
764 Experimental Thermal Analysis Data for Kinetic Computations. *Thermochim. Acta* **2014**,
765 *590*, 1–23. https://doi.org/10.1016/j.tca.2014.05.036.
766 (87) Fahmi, R.; Bridgwater, A. V.; Darvell, L. I.; Jones, J. M.; Yates, N.; Thain, S.; Donnison,
767 I. S. The Effect of Alkali Metals on Combustion and Pyrolysis of Lolium and Festuca
768 Grasses, Switchgrass and Willow. *Fuel* **2007**, *86* (10–11), 1560–1569.
769 https://doi.org/10.1016/j.fuel.2006.11.030.
770 (88) Deng, L.; Zhang, T.; Che, D. Effect of Water Washing on Fuel Properties, Pyrolysis and
771 Combustion Characteristics, and Ash Fusibility of Biomass. *Fuel Process. Technol.* **2013**,
772 *106*, 712–720. https://doi.org/10.1016/j.fuproc.2012.10.006.
773 (89) Lv, D.; Xu, M.; Liu, X.; Zhan, Z.; Li, Z.; Yao, H. Effect of Cellulose, Lignin, Alkali and
774 Alkaline Earth Metallic Species on Biomass Pyrolysis and Gasification. In *Fuel*
775 *Processing Technology*; 2010; Vol. 91, pp 903–909.
776 https://doi.org/10.1016/j.fuproc.2009.09.014.
777 (90) Collard, F. X.; Blin, J.; Bensakhria, A.; Valette, J. Influence of Impregnated Metal on the
778 Pyrolysis Conversion of Biomass Constituents. *J. Anal. Appl. Pyrolysis* **2012**, *95*, 213–
779 226. https://doi.org/10.1016/j.jaap.2012.02.009.
780 (91) Richardson, Y.; Motuzas, J.; Julbe, A.; Volle, G.; Blin, J. Catalytic Investigation of in Situ
781 Generated Ni Metal Nanoparticles for Tar Conversion during Biomass Pyrolysis. *J. Phys.*
782 *Chem. C* **2013**, *117* (45), 23812–23831. https://doi.org/10.1021/jp408191p.
783 (92) Sajid, M.; Zhao, X.; Liu, D. Production of 2,5-Furandicarboxylic Acid (FDCA) from 5-
784 Hydroxymethyl Furfural (HMF): A Recent Progress Focusing on the Chemical-Catalytic
785 Routes. *Green Chem.* **2018**. https://doi.org/10.1039/C8GC02680G.
786 (93) Zhang, Q.; Han, B.; Tang, X.; Heier, K.; Li, J. On the Mechanisms of Carbon Formation
787 Reaction on Ni (111) Surface. *J.* **2012**.
788 (94) Borel, L. D. M. S.; Lira, T. S.; Ribeiro, J. A.; Ataíde, C. H.; Barrozo, M. A. S. Pyrolysis of
789 Brewer's Spent Grain: Kinetic Study and Products Identification. *Ind. Crops Prod.* **2018**,
790 *121*, 388–395. https://doi.org/10.1016/j.indcrop.2018.05.051.
791 (95) Alonso, D. M.; Bond, J. Q.; Dumesic, J. A. Catalytic Conversion of Biomass to Biofuels.
792 *Green Chem.* **2010**, *12* (October), 1493–1513. https://doi.org/10.1039/c004654j.
793 (96) Garcia-Perez, M.; Chaala, A.; Pakdel, H. Characterization of Bio-Oils in Chemical
794 Families. *Biomass and* **2007**.
795 (97) Yoon, Y.; Rousseau, R.; Weber, R.; Mei, D. First-Principles Study of Phenol
796 Hydrogenation on Pt and Ni Catalysts in Aqueous Phase. *Chem. Soc.* **2014**.
797 (98) Patwardhan, P. R.; Satrio, J. A.; Brown, R. C.; Shanks, B. H. Influence of Inorganic Salts
798 on the Primary Pyrolysis Products of Cellulose. *Bioresour. Technol.* **2010**, *101* (12),
799 4646–4655. https://doi.org/10.1016/j.biortech.2010.01.112.

(99) Zhang, Z.; Zhao, Z. Production of 5-Hydroxymethylfurfural from Glucose Catalyzed by Hydroxyapatite Supported Chromium Chloride. *Bioresour. Technol.* **2011**, *102* (4), 3970–3972.
(100) Collard, F. X.; Bensakhria, A.; Drobek, M.; Volle, G.; Blin, J. Influence of Impregnated Iron and Nickel on the Pyrolysis of Cellulose. *Biomass and Bioenergy* **2015**, *80*, 52–62. https://doi.org/10.1016/j.biombioe.2015.04.032.
(101) Paine, J. B.; Pithawalla, Y. B.; Naworal, J. D. Carbohydrate Pyrolysis Mechanisms from Isotopic Labeling. Part 4. The Pyrolysis of d-Glucose: The Formation of Furans. *J. Anal. Appl. Pyrolysis* **2008**, *83* (1), 37–63. https://doi.org/10.1016/j.jaap.2008.05.008.
(102) Lin, Y.; Huber, G. The Critical Role of Heterogeneous Catalysis in Lignocellulosic Biomass Conversion. *Energy Environ. Sci.* **2009**.
(103) Dawes, G. J. S.; Scott, E. L.; Le Nôtre, J.; Sanders, J. P. M.; Bitter, J. H. Deoxygenation of Biobased Molecules by Decarboxylation and Decarbonylation - A Review on the Role of Heterogeneous, Homogeneous and Bio-Catalysis. *Green Chemistry*. 2015, pp 3231–3250. https://doi.org/10.1039/c5gc00023h.
(104) Stephanidis, S.; Nitsos, C.; Kalogiannis, K.; Iliopoulou, E. Catalytic Upgrading of Lignocellulosic Biomass Pyrolysis Vapours: Effect of Hydrothermal Pre-Treatment of Biomass. *Catal. Today* **2011**, *167* (1), 37–45.
(105) Williams, P. T.; Besler, S. The Influence of Temperature and Heating Rate on the Slow Pyrolysis of Biomass. *Renew. Energy* **1996**, *7* (3), 233–250. https://doi.org/10.1016/0960-1481(96)00006-7.
(106) Jacobsen, S. E.; Wyman, C. E. Cellulose and Hemicellulose Hydrolysis Models for Application to Current and Novel Pretreatment Processes. In *Applied Biochemistry and Biotechnology - Part A Enzyme Engineering and Biotechnology*; Humana Press: Totowa, NJ, 2000; Vol. 84–86, pp 81–96. https://doi.org/10.1385/ABAB:84-86:1-9:81.
(107) Nowakowski, D. J.; Jones, J. M.; Brydson, R. M. D.; Ross, A. B. Potassium Catalysis in the Pyrolysis Behaviour of Short Rotation Willow Coppice. *Fuel* **2007**, *86* (15), 2389–2402. https://doi.org/10.1016/j.fuel.2007.01.026.
(108) Lu, C.; Song, W.; Lin, W. Kinetics of Biomass Catalytic Pyrolysis. *Biotechnol. Adv.* **2009**, *27* (5), 583–587. https://doi.org/10.1016/j.biotechadv.2009.04.014.
(109) Li, J.; Yan, R.; Xiao, B.; Liang, D.; Lee, D. Preparation of Nano-NiO Particles and Evaluation of Their Catalytic Activity in Pyrolyzing Biomass Components†. *Energy & Fuels* **2007**, *333* (Part 2), 16–23.
(110) Li, J.; Yan, R.; Xiao, B.; Liang, D. T.; Lee, D. H. Preparation of Nano-NiO Particles and Evaluation of Their Catalytic Activity in Pyrolyzing Biomass Components. In *Energy and Fuels*; 2008; Vol. 22, pp 16–23. https://doi.org/10.1021/ef700283j.
(111) Temgire, M. K.; Joshi, S. S. Optical and Structural Studies of Silver Nanoparticles. *Radiat. Phys. Chem.* **2004**, *71* (5), 1039–1044. https://doi.org/10.1016/j.radphyschem.2003.10.016.
(112) Mandal, D.; Dash, S.; Das, B.; Chattopadhyay, S. Bio-Fabricated Silver Nanoparticles Preferentially Targets Gram Positive Depending on Cell Surface Charge. *Biomed.* **2016**.
(113) Chen, P.; Wu, Q. S.; Ding, Y. P. Facile Synthesis of Monodisperse Silver Nanoparticles by Bio-Template of Squama Inner Coat of Onion. *J. Nanoparticle Res.* **2008**, *10* (1), 207–213. https://doi.org/10.1007/s11051-007-9220-z.
(114) Liu, X.; Yang, P.; Jiang, Q. Size Effect on Melting Temperature of Nanostructured Drugs. *Mater. Chem. Phys.* **2007**, *103* (1), 1–4.

https://doi.org/10.1016/j.matchemphys.2007.01.014.
(115) Liu, W. J.; Jiang, H.; Yu, H. Q. Development of Biochar-Based Functional Materials: Toward a Sustainable Platform Carbon Material. *Chemical Reviews*. American Chemical Society November 25, 2015, pp 12251–12285. https://doi.org/10.1021/acs.chemrev.5b00195.
(116) Mullen, C. A.; Boateng, A. A.; Goldberg, N. M.; Lima, I. M.; Laird, D. A.; Hicks, K. B. Bio-Oil and Bio-Char Production from Corn Cobs and Stover by Fast Pyrolysis. *Biomass and Bioenergy* **2010**, *34* (1), 67–74. https://doi.org/10.1016/j.biombioe.2009.09.012.
(117) Liu, W. J.; Zeng, F. X.; Jiang, H.; Zhang, X. S. Preparation of High Adsorption Capacity Bio-Chars from Waste Biomass. *Bioresour. Technol.* **2011**, *102* (17), 8247–8252. https://doi.org/10.1016/j.biortech.2011.06.014.
(118) Yu, I. K.; Xiong, X.; Tsang, D. C.; Wang, L.; Hunt, A. J.; Song, H. C.; Shang, J.; Ok, Y. S.; Poon, C. S. Aluminium-Biochar Composites as Sustainable Heterogeneous Catalysts for Glucose Isomerisation in a Biorefinery. *Green Chem.* **2018**. https://doi.org/10.1039/C8GC02466A.
(119) Tan, X. fei; Liu, Y. guo; Gu, Y. ling; Xu, Y.; Zeng, G. ming; Hu, X. jiang; Liu, S. bo; Wang, X.; Liu, S. mian; Li, J. Biochar-Based Nano-Composites for the Decontamination of Wastewater: A Review. *Bioresource Technology*, 2016, *212*, 318–333. https://doi.org/10.1016/j.biortech.2016.04.093.
(120) He, R.; Peng, Z.; Lyu, H.; Huang, H.; Nan, Q.; Tang, J. Synthesis and Characterization of an Iron-Impregnated Biochar for Aqueous Arsenic Removal. *Sci. Total Environ.* **2018**, *612*, 1177–1186. https://doi.org/10.1016/j.scitotenv.2017.09.016.
(121) Tran, Q. H.; Nguyen, V. Q.; Le, A. T. Silver Nanoparticles: Synthesis, Properties, Toxicology, Applications and Perspectives. *Advances in Natural Sciences: Nanoscience and Nanotechnology*. IOP Publishing May 14, 2013, p 033001. https://doi.org/10.1088/2043-6262/4/3/033001.
(122) Kadirvelu, K.; Kavipriya, M.; Karthika, C.; Radhika, M.; Vennilamani, N.; Pattabhi, S. Utilization of Various Agricultural Wastes for Activated Carbon Preparation and Application for the Removal of Dyes and Metal Ions from Aqueous Solutions. *Bioresour. Technol.* **2003**, *87* (1), 129–132. https://doi.org/10.1016/S0960-8524(02)00201-8.
(123) Zhou, Y.; Gao, B.; Zimmerman, A. R.; Cao, X. Biochar-Supported Zerovalent Iron Reclaims Silver from Aqueous Solution to Form Antimicrobial Nanocomposite. *Chemosphere* **2014**, *117* (1), 801–805. https://doi.org/10.1016/j.chemosphere.2014.10.057.

881 **Table 1.** Proximate and ultimate analysis of brewer's spent grain

Ultimate Analysis (dry wt%)	
C	50.57 ± 2.01
H	6.46 ± 0.32
N	6.41 ± 0.23
O*	36.02 ± 1.13
S	0.56 ± 0.04
Proximate Analysis (wt%, dry basis)	
Volatile Matter	80.07 ± 1.40
Fixed Carbon	17.18 ± 0.26
Ash	2.75 ± 0.03

*by difference

882
883
884 **Table 2.** Product distribution for raw and Ag-impregnated BSG

	Mass Fraction Pyrolyzed	**Mass Fraction Oxidized**	**Inorganic Yield**
Raw BSG	0.805 ± 0.010	0.171 ± 0.003	0.024 ± 0.005
Ag-Soaked BSG	0.813 ± 0.006	0.107 ± 0.003	0.080 ± 0.004
	Condensable Yield (g/kg_{BSG})	**Pyrolysis Gas Yield (g/kg_{BSG})**	**Silver Yield (g/kg_{BSG})**
Raw BSG	190.5 ± 6.2	614.5 ± 17.6	(not applicable)
Ag-Soaked BSG	178.4 ± 2.5	643.8 ± 14.8	5.59 ± 0.98

885
886
887
888 **Table 3.** Relative (Rel.) change in amount of pyrolysis gases evolved due to impregnation of
889 silver in brewer's spent grain

Integrated MS Area	H_2 m/z = 2	CH_4 m/z = 16	C_2H_2 m/z = 26	C_2H_4 m/z = 27	C_2H_6 m/z = 30	CO_2 m/z = 44
Raw BSG	7.856E-05	2.243E-04	4.571E-05	1.811E-04	2.097E-05	7.531E-04
Ag BSG	8.200E-04	2.159E-04	4.127E-05	1.849E-04	3.433E-05	9.183E-04
Rel. Change:	944%	-4%	-10%	2%	64%	22%

890
891
892
893

Table 4. Bio-oil compounds identified by GC-MS from raw and impregnated biomass pyrolysis at 10°C/min up to 500°C. Quantitative yields are show for compounds for which calibration curves were available.

Retention Time (min)	Compound	CAS Number	Raw BSG			Ag soaked BSG		
			Area (% chromatogram peaks)	Normalized peak area	Yield (g/kg_{BSG})	Area (% chromatogram peaks)	Normalized peak area	Yield (g/kg_{BSG})
8.7	2-hexene	592-43-8	5.0%	66140			n.d.	
8.8	2(3H)-furanone	20825-71-2	11.0%	153475		10.0%	98313	
11.6	2-Furancarboxaldehyde	98-01-1		n.d.		21.0%	210306	35.1
15.9	2,5-hexanedione	110-13-4	3.0%	36570	19.5	1.0%	14845	7.9
16.3	Phenol	108-95-2	2.0%	25019	2.5		n.d.	
17.5	2-Acetylfuran	1192-62-7	1.0%	12711			n.d.	
19.7	2-methylpropanal	78-84-2		n.d.		9.0%	86965	
22.7	2,6-dimethoxyphenol (syringol)	91-10-1	2.0%	25019	2.5		n.d.	
23.3	3-methyl-1,2-cyclopentanedione	765-70-8	2.0%	31678	5.9		n.d.	
25.2	2-propenyl ester-Acetic acid	591-87-7	5.0%	74819		4.0%	41550	
25.6	2-methylbutyraldehyde	96-17-3	5.0%	206240		8.0%	77012	
27.7	p-cresol	106-44-5	0.3%	4140		2.0%	15016	1.4
35.7	5-hydroxymethylfurfural	67-47-0	6.0%	80858		2.0%	16423	
46.3	fluorene	86-73-7		n.d.		1.0%	5532	0.19
49.3	anthracene	120-12-7	3.0%	34828	6.2		n.d.	
55.3	pyrene	129-00-0	6.0%	7908	1.3		n.d.	
66.5	hexadecanoic acid	57-10-3	1.0%	17051		4.0%	35067	

n.d. = not detected

Table 5. Thermogravimetric results of pyrolysis of raw un-soaked BSG, water-soaked BSG, and silver-impregnated BSG biomass samples.

	Peak DTG					
	Peak 1 T (°C)	Peak 1 Rate (1/s)	Peak 2 T (°C)	Peak 2 Rate (1/s)	Peak 3 T (°C)	Peak 3 Rate (1/s)
	5 °C/min					
Raw BSG	194	2.18E-04	272	5.21E-04	328	5.18E-04
Ag BSG	-	-	272	5.19E-04	321	5.21E-04
Water Soaked BSG	-	-	281	6.93E-04	335	5.55E-04
	10 °C/min					
Raw BSG	202	3.13E-04	285	9.72E-04	338	9.42E-04
Ag BSG	-	-	278	1.01E-03	327	1.01E-03
Water Soaked BSG	-	-	289	1.35E-03	346	1.01E-03
	25 °C/min					
Raw BSG	215	9.36E-04	293	2.61E-03	341	2.54E-03
Ag BSG	-	-	289	2.42E-03	337	2.42E-03
Water Soaked BSG	-	-	299	3.50E-03	355	2.58E-03
	50 °C/min					
Raw BSG	223	1.71E-03	299	5.12E-03	352	4.97E-03
Ag BSG	-	-	294	4.86E-03	346	4.83E-03
Water Soaked BSG	-	-	309	6.72E-03	357	5.12E-03

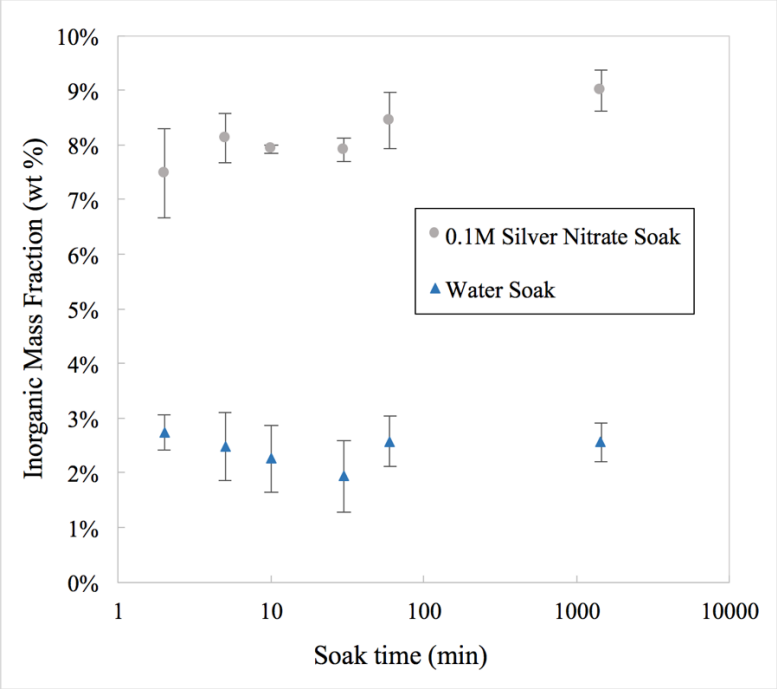

Figure 1. Change in inorganic fraction of biomass versus soak time in 0.1M $AgNO_3$ solution and in water.

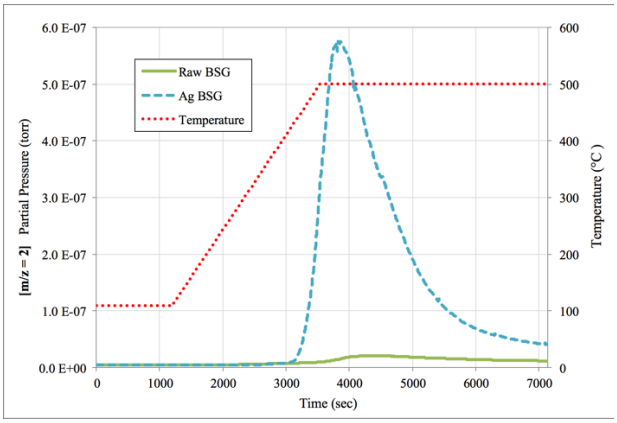

a. Hydrogen (m/z = 2) evolved from BSG pyrolysis

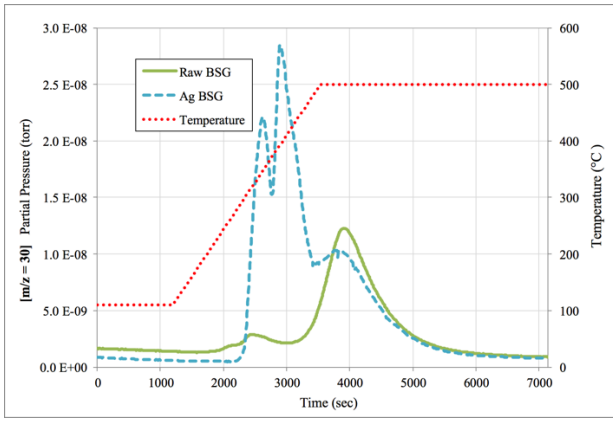

b. Ethane (m/z = 30) evolved from BSG pyrolysis

Figure 2. Mass Spectra of (a) H_2 and (b) C_2H_6 evolved during pyrolysis of raw and silver-impregnated BSG (spectra of all monitored gases as function of time (including isothermal hold step) and temperature available in Supplemental Information)

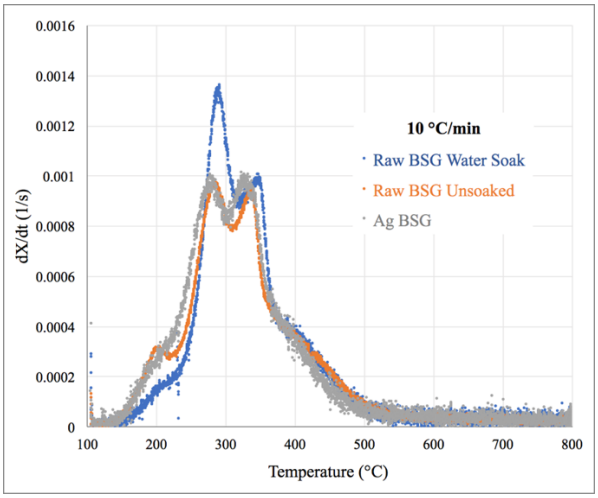

Figure 3. Representative DTG curve for pyrolysis of raw, soaked and Ag-impregnated BSG pyrolyzed at 10 °C/min (additional heating rate plots available in SI)

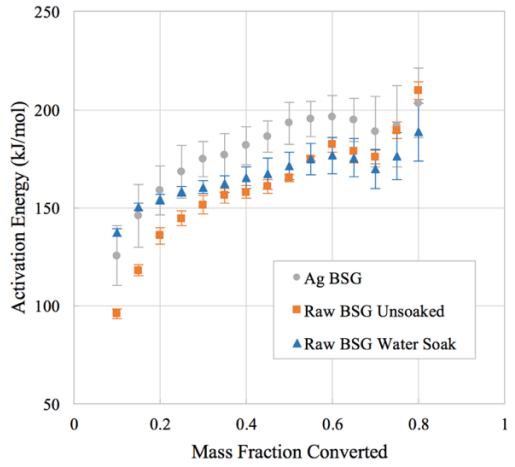

a. Activation energy as a function of mass fraction converted calculated by DAEM

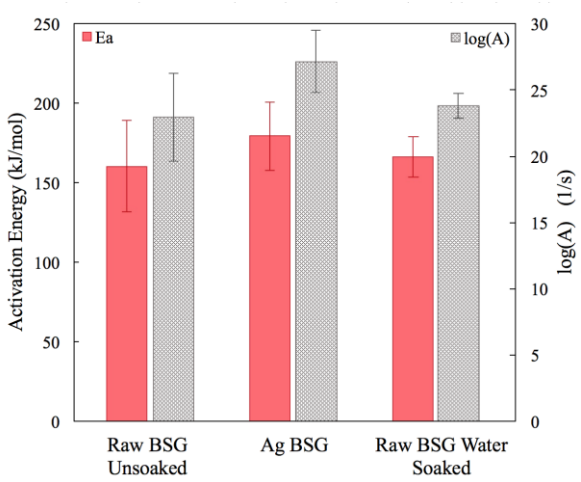

b. Average activation energy and pre-exponential factors calculated by DAE

Figure 4. Activation energy of pyrolysis of raw un-soaked BSG, water-soaked BSG, and silver-impregnated BSG biomass samples.

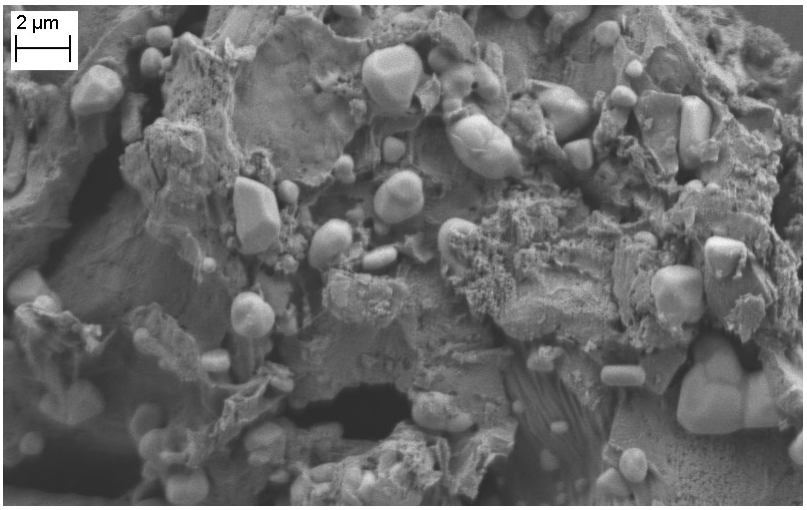

Figure 5. SEM image of calcined silver-impregnated brewer's spent grain (scale bar represents 2 µm)